UV radiation and CH_4 gas detection with a single ZnO:Pd nanowire

O. Lupan,[a,b,c,d], R. Adelung,[b] V. Postica,[c] N. Ababii,[c] L. Chow,[d] B. Viana,[a] T. Pauporté[a]

[a] PSL Research University, Chimie ParisTech-CNRS, Institut de Recherche de Chimie Paris, 11 rue P. et M. Curie, 75005 Paris, France
[b] Functional Nanomaterials, Institute for Materials Science, Christian Albrechts University of Kiel, 24143 Kiel, Germany
[c] Department of Microelectronics and Biomedical Engineering, Technical University of Moldova, 168 Stefan cel Mare Blvd., MD-2004, Chisinau, Republic of Moldova
[d] Department of Physics, University of Central Florida, Orlando, FL 32816-2385, USA

ABSTRACT

There is an increasing demand for sensors to monitor environmental levels of ultraviolet (UV) radiation and pollutant gases. In this work, an individual nanowire of Pd modified ZnO nanowire (ZnO:Pd NW) was integrated in a nanosensor device for efficient and fast detection of UV light and CH_4 gas at room temperature. Crystalline ZnO:Pd nanowire/nanorod arrays were synthesized onto fluorine doped tin oxide (FTO) substrates by electrochemical deposition (ECD) at relative low-temperatures (90 °C) with different concentrations of $PdCl_2$ in electrolyte solution and investigated by SEM and EDX. Nanodevices were fabricated using dual beam focused electron/ion beam (FIB/SEM) system and showed improved UV radiation response compared to pristine ZnO NW, reported previously by our group. The UV response was increased by one order in magnitude (≈ 11) for ZnO:Pd NW. Gas sensing measurements demonstrated a higher gas response and rapidity to methane (CH_4 gas, 100 ppm) at room temperature, showing promising results for multifunctional applications. Also, due to miniature size and ultra-low power consumption of these sensors, it is possible to integrate them into portable devices easily, such as smartphones, digital clock, flame detection, missile lunching and other smart devices .

Keywords: ZnO, nanosensor, methane, UV light, multifunctional.

1. INTRODUCTION

UV light is known to be beneficial for people at low dose due to production of vitamin D, which is very important for immunoregulatory processes [1-2]. Low vitamin D status is extremely common nowadays and may lead to the development of different diseases, such as rickets, psoriasis, eczema, and *etc.* [1]. Moderate UV radiation exposure can prevent many of these diseases, as demonstrated by clinical investigations [2]. On the other hand, long exposure of ultraviolet B rays (UVB, λ = 280 – 315 nm), may results in different acute and chronic diseases of the skin, including skin cancer [3]. In clinical conditions, the UV exposure takes place under control of medical supervision, thus, prolonged exposure to UV radiation is considerably reduced. For people who are long time exposed to UV radiation from sunlight, the risk of skin diseases is higher. The CH_4 gas monitoring is also very important for the purpose of safety in homes, industries and mines [4]. At a concentration of 5-14% concentration of CH_4 gas in air, methane is highly explosive, it is a frequent cause of disasters in homes and industries [4].

Therefore, it is necessary to develop a multifunctional miniature device able to continuously monitor the time exposure to UV light and concentration of CH_4 in air. In this work, we present a nanosensor device based on an individual ZnO:Pd NW, which can perform simultaneously several tasks at the same operating conditions, i.e. the detection of UV light (λ = 365 nm) and CH_4 gas in small concentrations (100 ppm). Multifunctional operation is possible at room temperature operation due to the nanometric size of sensing material [5], thus the necessity of micro-heater element and thermometer plate is avoided resulting in ultra-low power detection of UV light and CH_4 gas with the same sensing material.

Oxide-based Materials and Devices VIII, edited by Ferechteh H. Teherani, David C. Look, David J. Rogers, Proc. of SPIE Vol. 10105, 101051Y · © 2017 SPIE
CCC code: 0277-786X/17/$18 · doi: 10.1117/12.2249841

2. MATERIAL SYNTHESIS AND DEVICE STRUCTURES FABRICATION.

ZnO NW arrays were prepared by an electrochemical technique developed by some of us [6-8]. The ZnO:Pd NW arrays were electrodeposited on FTO/glass substrates with a resistance of 10 Ω/square at relatively low temperature (90°C) using zinc chloride and molecular oxygen as the growth precursors. The doping was achieved by adding a small amount of $PdCl_2$ (Alfa Aesar) in the electrolyte solution with different concentrations (0.5 – 1.5 μM). More details on morphological, structural, chemical and optical properties are presented in our previous works [9-10]. In the present work, only the UV and CH_4 sensing properties are presented. After synthesis, the samples were annealed in air at 250°C for a period of 12 h. The morphological and chemical (EDX) properties were studied as previously reported [9, 11-15]. The gas sensing measurements and UV photodetection were performed under the same experimental conditions as in [5]. The nanosensor devices were fabricated using FIB/SEM systems by the same procedure as described by Lupan *et al.* [5, 11, 16-17]. The electrical measurements were continuously monitored and collected using a computer controlled Keithley 2400 sourcemeter through a LabView software (National Instruments) applying different bias voltages. The investigations were performed in a quasi-steady state.

3. RESULTS AND DISCUSSIONS

Figure 1(a) shows a typical SEM image of two-terminal nanosensor device based on an individual ZnO:Pd NW (0.8 μM $PdCl_2$) with diameter of 100 nm. The substrates were SiO_2 (350 nm)/Si chip with pre-patterned Au/Cr electrodes [18]. The ZnO:Pd NWs were released from FTO substrate and then transferred to substrate chip [5, 11]. Using a FIB/SEM system, two platinum (Pt) rigid contacts from platinum (Pt) were formed at both ends of the NWs for contacting them to the Au electrodes. Series of devices were fabricated on individual ZnO NWs with a diameter (D) ≈ 100 nm and different concentrations of $PdCl_2$ in the electrolyte solution (0.5 – 1.5 μM $PdCl_2$), in order to investigate the influence of Pd on UV radiation and CH_4 gas response. It is well-known that type of NWs contacts affect the current-voltage (*I-V*) characteristic of device, as well as UV and gas sensing properties, which is a key factor for understanding of transport mechanism in NW [19-20]. The all devices fabricated in this work with Pt-ZnO:Pd-Pt structure demonstrated non-linear *I-V* characteristics in both regions of applied bias, i.e. negative and positive. Figure 1(b) shows the typical *I-V* curve of the nanosensor presented in Fig. 1(a). This may indicate the formation of asymmetric Schottky contacts at both ends of NWs, i.e. metal (Pd) – ZnO:Pd contacts, which was demonstrated experimentally by many authors and is cause of higher work function of Pt compared to electron affinity of ZnO [20-21].

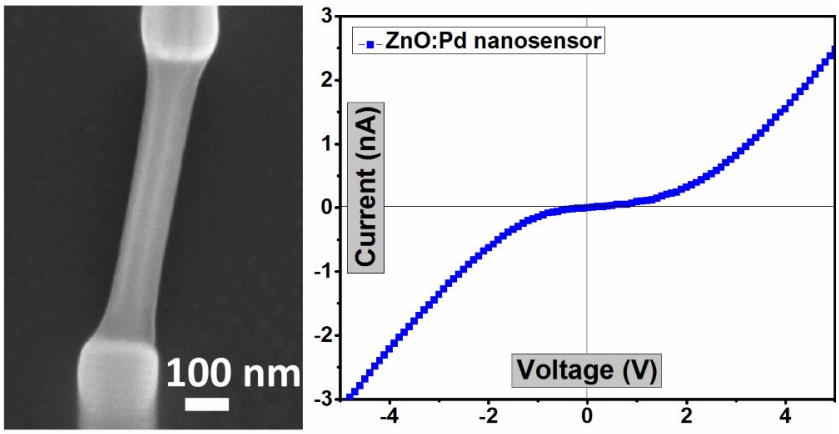

Figure 1. (a) SEM images of a nanosensor based on an individual ZnO:Pd nanowire with diameter of 100 nm. (b) Current – voltage characteristics of the nanosensor device.

Next, the UV sensing properties of nanosensors based on a single ZnO:Pd NW is discussed. Figure 2(a-d) shows the dynamic UV response of nanosensors based on ZnO:Pd NW from samples with different concentrations of $PdCl_2$ in electrolyte solution (μM). As can be observed, at relatively low concentration of $PdCl_2$ (0.5 μM, see Fig. 2(a)), the nanosensor shows unstable electrical baseline with a continuous drift, as well as slow response and recovery. This is not suitable for real applications and requires additional electrical schemes, which leads to increase of the final device cost and size. Compared to pristine ZnO NW with the same diameter (100 nm) reported in a previous work [22], the UV response of ZnO:Pd NW (with 0.5 μM $PdCl_2$) is about 1.24 time higher, showing an increased response. Increasing $PdCl_2$ concentration to 0.8 μM results in a further increase of UV response to $I_{uv}/I_{dark} \approx 14$, which is about 11 times higher than for pristine ZnO NW (see Fig. 2(b)). Beside this increase in UV response, the improvement in the stability was observed with good recovery to the initial baseline. However, further increase in $PdCl_2$ concentration leads to a gradual degradation of UV response (see Fig. 2(e)). While nanosensor based on ZnO:Pd NW (1.25 μM $PdCl_2$) possesses the same good stability and comparable rapidity as the ZnO:Pd NW (0.8 μM $PdCl_2$, see Fig. 2(b) and Fig. 2(c)), the nanosensor based on ZnO:Pd NW (1.5 μM $PdCl_2$) showed high instability (see Fig. Fig. 2(d)).

In order to evaluate the UV photodetection rapidity of nanosensors, the bi-exponential fitting was used to determine the time constants for rising (τ_{r1} and τ_{r2}) and decaying (τ_{d1} and τ_{d2}) photocurrent [5, 23]. The results are plotted in Fig. 2(f). A decrease tendency is observed for all the time constants. The decrease in value of rapid components of photocurrent (τ_{r1} and τ_{d1}) by increase of concentration of $PdCl_2$ in electrolyte solution can be observed. These components are correlated to the rapid change in the concentration of charge carriers during the switching of UV light [23-24]. The slow components (τ_{r2} and τ_{d2}) of photoresponse curves are related to photodesorption/adsorption processes of oxygen species onto surface of NW [23-24], and showed the same tendency of decrease values with increasing $PdCl_2$ concentration in electrolyte solution (see Fig. 2(f)).

Responsivity (R) and internal photoconductive gain (G) were calculated using the following equations [25-27]:

$$R = \frac{I_{ph}}{P_{opt}} = \eta\left(\frac{q\lambda}{hc}\right)G \tag{1}$$

$$G \cong \frac{1}{L^2}\tau\mu_e V \tag{2}$$

where I_{ph} is the photocurrent, P_{opt} is the incident optical power of the UV source (15 mW/cm^2), η is the quantum efficiency, h is the Planck's constant, c is the speed of light, λ is the wavelength of UV light (365 nm), L is the interelectrode spacing, μ_e is the electron mobility, τ is the photocarrier lifetime and V is the applied bias. The estimated values for Responsivity R are 115, 185, 171 and 123 for 0.5, 0.8, 1.25 and 1.5 μM of $PdCl_2$, respectively. While the estimated values for i-photoconductive gain G is 33, 54, 50 and 36, respectively. This indicates the presence of internal photoconductive gain for fabricated nanosensors and can be due to small interelectrode spacing in fabricated devices (see Fig. 1(a)) [26-27].

The gas sensing measurements to CH_4 gas demonstrated high gas response at room temperature. Figure 3 shows the dynamic gas response to 100 ppm for individual ZnO:Pd NW grown using 0.5 and 0.8 μM of $PdCl_2$. Several pulses of gas were applied in order to check the repeatability of the nanosensors response. As can be observed, the ZnO:Pd NW grown using 0.5 μM of $PdCl_2$ showed higher gas response to CH_4 gas, while by increasing the $PdCl_2$ concentration, the decrease in response is observed. The calculated gas response is ≈ 5.7 and ≈ 1.8, for nanosensors grown using 0.5 and 0.8 μM of $PdCl_2$, respectively. The response times (τ_r) and recovery times (τ_d) were also estimated from the dynamic response of nanosensors. The obtained results are τ_r = 6.2 s and τ_d = 48 s for 0.5 μM $PdCl_2$, and τ_r = 8.1 s and τ_d = 123 s for 0.8 μM $PdCl_2$. Due to low currents in the dark and exposure in air, the power consumption of such devices is very low (1-10 nW).

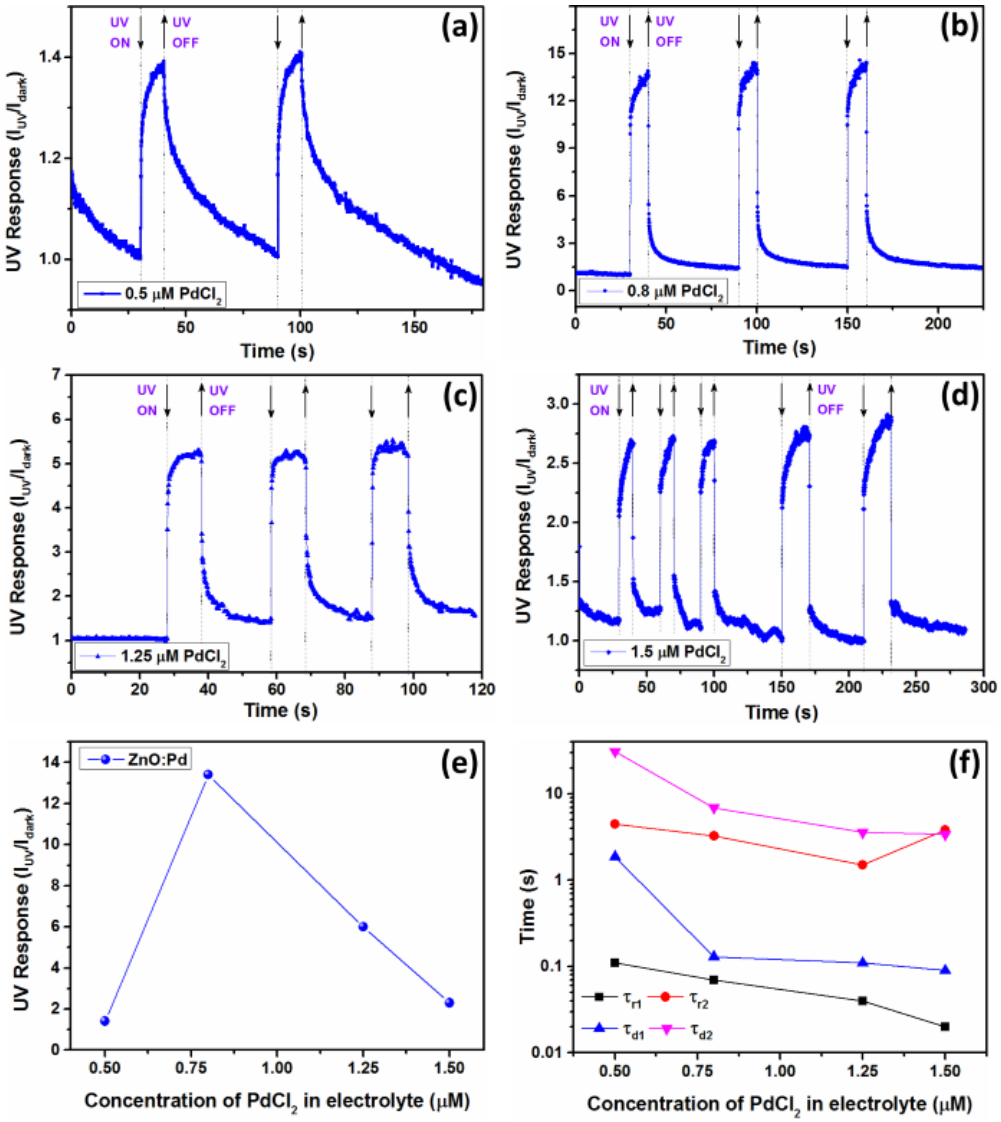

Figure 2. Dynamic UV response of nanosensor at room temperature based on individual ZnO:Pd NW grown in electrolyte solution with the following concentration of $PdCl_2$: (a) 0.5 μM; (b) 0.8 μM; (c) 1.25 μM; (d) 1.5 μM. (e) UV radiation response and (f) the calculated rise and decay times versus concentration of $PdCl_2$ in electrolyte solution.

The mechanism for methane gas detection can be explained as follows. Under exposure to air, the adsorption of oxygen molecules takes place onto the surface of NW [28]:

$$O_2(g) \leftrightarrow O_2(ads) + e^- \leftrightarrow O_2^-(ads) \quad (3)$$

$$V_0 + \frac{1}{2}O_2(g) + 2e^- \leftrightarrow O^{2-}(ads) \quad (4)$$

where V_0 is the surface oxygen vacancy. Also, due to the presence of Pd nanoparticles [9] the oxygen spillover process is enhanced [29-30].

$$2Pd + O_2(g) \leftrightarrow 2Pd:O(ads) \quad (5)$$

$$O(ads) + e^- \leftrightarrow O^-(ads) \quad (6)$$

Therefore, resulting in a higher coverage with oxygen species and a higher degree of electron withdrawal from the ZnO NW, i.e. higher modulation of the conduction channel (gas response) [5, 30]. Then under exposure to CH_4, the surface reaction process takes place and can be expressed as follows [28-29, 31]:

$$CH_4(g) + 2O_2^-(ads) \rightarrow CO_2(g) + 2H_2O(g) + 4e^- \quad (7)$$

$$CH_4(g) + 4O^-(ads) \rightarrow CO_2(g) + 2H_2O(g) + 4e^- \quad (8)$$

$$CH_4(g) + 2O^{2-}(ads) \rightarrow CO_2(g) + 2H_2O(g) + 4e^- \quad (9)$$

In results of electron donating the width of conduction channel is extended [5]. Thus, the enhanced CH_4 response of ZnO:Pd NW compared to pristine ZnO NW can be explained based on the presence of Pd nanoparticles at the surface of ZnO:Pd NWs [9].

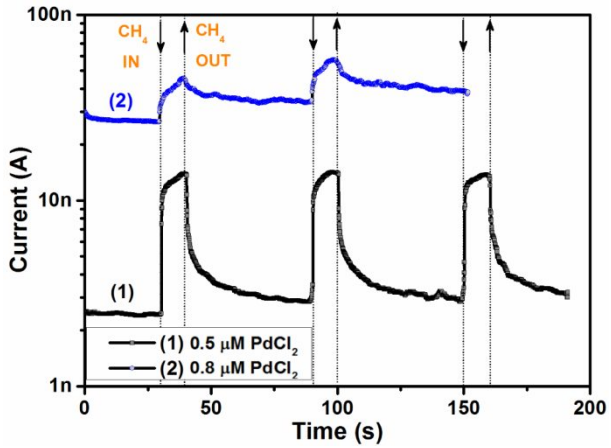

Figure 3. Dynamic gas response at room temperature to 100 ppm of CH_4 gas for individual ZnO:Pd NW grown in electrolyte solution using 0.5 μM and 0.8 μM of $PdCl_2$. The applied bias voltage was 1 V.

The enhanced UV response can also be explained based on catalytic properties of Pd nanoparticles, i.e. higher oxygen coverage due to higher catalytic properties of oxygen molecules dissociation of Pd nanoparticles compared to ZnO surface [30]. Under UV illumination, the electron-hole (e^- – h^+) pairs are generated and are separated by built-in electric field in the electron depleted region created by ionization of oxygen species at the surface of ZnO [5]. The photo-generated electrons will contribute to an increase in the photocurrent value through the device, while the photo-generated holes will migrate to the surface to discharge adsorbed oxygen ions from the surface of ZnO NW ($2h^+ + O^{2-}(ads) \rightarrow \frac{1}{2}O_2(g)$) [5]. The improved UV detection speed is due to faster degree of the slow reactions (photodesorption/adsorption processes of oxygen species onto surface of NW) due to higher catalytic effect of Pd nanoparticles [30].

5. CONCLUSIONS

In this work we demonstrate that individual ZnO:Pd NW with diameter ≈ 100 nm can be successfully integrated into nanodevices using FIB/SEM system. Fabricated multifunctional nanodevices show possibility to perform several tasks, i.e. fast detection of UV light and highly sensitive detection of CH_4 gas at low concentrations at the same operation conditions (at room temperature). The optimal $PdCl_2$ concentration for highest UV radiation response (≈ 14) is 0.8 μM, while for highest CH_4 gas response (≈ 5.7) the concentration is 0.5 μM. Both types of sensors demonstrated good stability of electrical baseline and excellent repeatability. For the nanodevices operating at room temperature the response time to CH_4 is relatively fast (τ_r = 8.1 s). Such nanodevices can be easily integrated into smart devices for continuous monitoring of UV radiation and CH_4 gas for safety purposes due to high performances and low power consumption.

Acknowledgements

Dr. Lupan gratefully acknowledges CNRS Council for support as expert scientist at IRCP Chimie ParisTech, Paris. Professor Dr. Adelung (CAU, Kiel, Germany) is acknowledged for fruitful discussions and for his help with FIB/SEM experiments. This work was partially financially supported by the STCU under the Grant no. 5989.

References

[1]. Binkley, N.; Novotny, R.; Krueger, D.; Kawahara, T.; Daida, Y. G.; Lensmeyer, G.; Hollis, B. W.; Drezner, M. K., Low Vitamin D Status Despite Abundant Sun Exposure. J. Clin. Endocr. Metab. , 92, 2130-2135 (2007).

[2]. Hart, P. H.; Gorman, S.; Finlay-Jones, J. J., Modulation of the Immune System by Uv Radiation: More Than Just the Effects of Vitamin D? Nat. Rev. Immunol. , 11, 584-596 (2011).

[3]. de Gruijl, F. R., Skin Cancer and Solar Uv Radiation. Eur. J. Cancer , 35, 2003-2009 (1999).

[4]. Sun, P.; Jiang, Y.; Xie, G.; Du, X.; Hu, J., A Room Temperature Supramolecular-Based Quartz Crystal Microbalance (Qcm) Methane Gas Sensor. Sens. Actuators B , 141, 104-108 (2009).

[5]. Lupan, O.; Cretu, V.; Postica, V.; Ahmadi, M.; Cuenya, B. R.; Chow, L.; Tiginyanu, I.; Viana, B.; Pauporté, T.; Adelung, R., Silver-Doped Zinc Oxide Single Nanowire Multifunctional Nanosensor with a Significant Enhancement in Response. Sens. Actuators B , 223, 893-903 (2016).

[6]. Pauporté, T.; Bataille, G.; Joulaud, L.; Vermersch, F. J., Well-Aligned Zno Nanowire Arrays Prepared by Seed-Layer-Free Electrodeposition and Their Cassie−Wenzel Transition after Hydrophobization. J. Phys. Chem. C , 114, 194-202 (2010).

[7]. Lupan, O.; Pauporté, T.; Viana, B., Low-Temperature Growth of Zno Nanowire Arrays on P-Silicon (111) for Visible-Light-Emitting Diode Fabrication. J. Phys. Chem. C , 114, 14781-14785 (2010).

[8]. Pauporte, T.; Pelle, F.; Viana, B.; Aschehoug, P., Luminescence of Nanostructured Eu3+/Zno Mixed Films Prepared by Electrodeposition. Journal of Physical Chemistry C, 111, 15427-15432 (2007).

[9]. Lupan, O.; Postica, V.; Pauporté, T.; Adelung, R., Synthesis of Pd Functionalized Zno Nanowire Arrays for Integration in Nanosensor Devices J. Mater. Chem. A (2017).

[10]. Pauporté, T.; Lupan, O.; Zhang, J.; Tugsuz, T.; Ciofini, I.; Labat, F. d. r.; Viana, B., Low-Temperature Preparation of Ag-Doped Zno Nanowire Arrays, Dft Study, and Application to Light-Emitting Diode. ACS Appl. Mater. Interfaces , 7, 11871-11880 (2015).

[11]. Lupan, O.; Postica, V.; Cretu, V.; Wolff, N.; Duppel, V.; Kienle, L.; Adelung, R., Single and Networked Cuo Nanowires for Highly Sensitive P-Type Semiconductor Gas Sensor Applications. Phys. Status Solidi RRL , 10, 260 - 266 (2016).

[12]. Cretu, V.; Postica, V.; Mishra, A. K.; Hoppe, M.; Tiginyanu, I.; Mishra, Y. K.; Chow, L.; De Leeuw, N. H.; Adelung, R.; Lupan, O., Synthesis, Characterization and Dft Studies of Zinc-Doped Copper Oxide Nanocrystals for Gas Sensing Applications. J. Mater. Chem. A , 4, 6527-6539 (2016).

[13]. Lupan, O.; Viana, B.; Cretu, V.; Postica, V.; Adelung, R.; Pauporté, T., Low Temperature Preparation of Ag-Doped Zno Nanowire Arrays for Sensor and Light-Emitting Diode Applications. Proc. SPIE 2016, 9749, 97490U (2016).

[14]. Perez-Casero, R.; Gutierrez-Llorente, A.; Pons-Y-Moll, O.; Seiler, W.; Defourneau, R. M.; Defourneau, D.; Millon, E.; Perriere, J.; Goldner, P.; Viana, B., Er-Doped Zno Thin Films Grown by Pulsed-Laser Deposition. Journal of Applied Physics , 97 (2005).
[15]. Lupan, O.; Pauporte, T.; Viana, B., Low-Temperature Growth of Zno Nanowire Arrays on P-Silicon (111) for Visible-Light-Emitting Diode Fabrication. Journal of Physical Chemistry C , 114, 14781-14785 (2010).
[16]. Paulowicz, I., et al., Three-Dimensional Sno_2 Nanowire Networks for Multifunctional Applications: From High-Temperature Stretchable Ceramics to Ultraresponsive Sensors. Adv. Electron. Mater. , 1, 1500081 (2015).
[17]. Hölken, I.; Neubüser, G.; Postica, V.; Bumke, L.; Lupan, O.; Baum, M.; Mishra, Y. K.; Kienle, L.; Adelung, R., Sacrificial Template Synthesis and Properties of 3d Hollow-Silicon Nano-and Microstructures. ACS Appl. Mater. Interfaces , 8, 20491-20498 (2016).
[18]. Lupan, O.; Cretu, V.; Deng, M.; Gedamu, D.; Paulowicz, I.; Kaps, S. r.; Mishra, Y. K.; Polonskyi, O.; Zamponi, C.; Kienle, L., Versatile Growth of Freestanding Orthorhombic A-Molybdenum Trioxide Nano-and Microstructures by Rapid Thermal Processing for Gas Nanosensors. J. Phys. Chem. C , 118, 15068-15078 (2014).
[19]. Zhang, Z.; Yao, K.; Liu, Y.; Jin, C.; Liang, X.; Chen, Q.; Peng, L. M., Quantitative Analysis of Current–Voltage Characteristics of Semiconducting Nanowires: Decoupling of Contact Effects. Adv. Funct. Mater. 2007, 17, 2478-2489 (2013).
[20]. Das, S. N.; Moon, K.-J.; Kar, J. P.; Choi, J.-H.; Xiong, J.; Lee, T. I.; Myoung, J.-M., Zno Single Nanowire-Based Uv Detectors. Appl. Phys. Lett., 97, 022103 (2010).
[21]. Wang, Z. L.; Song, J., Piezoelectric Nanogenerators Based on Zinc Oxide Nanowire Arrays. Science , 312, 242-246 (2006).
[22]. Lupan, O.; Chai, G.; Chow, L.; Emelchenko, G. A.; Heinrich, H.; Ursaki, V. V.; Gruzintsev, A. N.; Tiginyanu, I. M.; Redkin, A. N., Ultraviolet Photoconductive Sensor Based on Single Zno Nanowire. Phys. Status Solidi A , 207, 1735-1740 (2010).
[23]. Postica, V.; Hölken, I.; Schneider, V.; Kaidas, V.; Polonskyi, O.; Cretu, V.; Tiginyanu, I.; Faupel, F.; Adelung, R.; Lupan, O., Multifunctional Device Based on Zno:Fe Nanostructured Films with Enhanced Uv and Ultra-Fast Ethanol Vapour Sensing. Mater. Sci. Semicon. Proc. , 49, 20-33 (2016).
[24]. Zhang, D. H., Adsorption and Photodesorption of Oxygen on the Surface and Crystallite Interfaces of Sputtered Zno Films. Mater. Chem. Phys. , 45, 248-252 (1996).
[25]. Xu, K.; Wang, Z.; Wang, F.; Huang, Y.; Wang, F.; Yin, L.; Jiang, C.; He, J., Ultrasensitive Phototransistors Based on Few-Layered Hfs_2. Adv. Mater. , 27, 7881-7887 (2015).
[26]. Peng, S.-M.; Su, Y.-K.; Ji, L.-W.; Wu, C.-Z.; Cheng, W.-B.; Chao, W.-C., Zno Nanobridge Array Uv Photodetectors. J. Phys. Chem. C , 114, 3204-3208 (2010).
[27]. Soci, C.; Zhang, A.; Xiang, B.; Dayeh, S. A.; Aplin, D. P. R.; Park, J.; Bao, X. Y.; Lo, Y. H.; Wang, D., Zno Nanowire Uv Photodetectors with High Internal Gain. Nano Lett. , 7, 1003-1009 (2007).
[28]. Chai, G. Y.; Lupan, O.; Rusu, E. V.; Stratan, G. I.; Ursaki, V. V.; Şontea, V.; Khallaf, H.; Chow, L., Functionalized Individual Zno Microwire for Natural Gas Detection. Sens. Actuators A , 176, 64-71 (2012).
[29]. Basu, P. K.; Jana, S. K.; Saha, H.; Basu, S., Low Temperature Methane Sensing by Electrochemically Grown and Surface Modified Zno Thin Films. Sens. Actuators B , 135, 81-88 (2008).
[30]. Kolmakov, A.; Klenov, D. O.; Lilach, Y.; Stemmer, S.; Moskovits, M., Enhanced Gas Sensing by Individual Sno_2 Nanowires and Nanobelts Functionalized with Pd Catalyst Particles. Nano Lett. , 5, 667-673 (2005).
[31]. Zhou, Q.; Chen, W.; Xu, L.; Peng, S., Hydrothermal Synthesis of Various Hierarchical Zno Nanostructures and Their Methane Sensing Properties. Sensors, 13 (2013).